Design of Linear Induction Drives by Field Analysis and Finite-Element Techniques

GRAHAM E. DAWSON, MEMBER, IEEE, ANTHONY R. EASTHAM, SENIOR MEMBER, IEEE, JACEK F. GIERAS, MEMBER, IEEE, RAYMOND ONG, AND KRISNAMOORTHY ANANTHASIVAM

Abstract—**Two-dimensional field and finite-element analyses are complementary in evaluating the performance of single-sided linear induction machines, and can be used to develop a machine design for a given drive application. Electromagnetic analysis leads to an equivalent circuit of the machine with speed- and frequency-dependent parameters, in which top cap geometry, core hysteresis and saturation, skin effect, eddy current reaction, and both transverse-edge and longitudinal-end effects can be included. Finite-element analysis provides detailed information on the magnetic field distribution to aid in machine design.**

I. Introduction

As TRANSPORTATION drives, linear induction motors (LIM's) are finding their first applications in transit vehicles such as Urban Transportation Development Corporation's (UTDC) steerable-axle trucked intermediate-capacity transit system, now operational in Scarborough, ON, and being implemented in Vancouver, BC, Canada, and Detroit, MI; in the WEDWAY People Mover in Orlando, FL, and at the Houston Airport, Houston, TX; in the magnetically suspended Advanced Transit Shuttle link at the Birmingham Airport in England; and in the mini-subway (LM-1) and HSST systems being developed in Japan. Photographs of four of these vehicles are shown in Fig. 1.

Operating experience with these systems is generating a better understanding of the unique features of LIM's and of the trade-offs in their implementation (i.e., guaranteed thrust and braking performance, improved grade-climbing capability, and lower maintenance costs against reduced operational efficiency as compared with rotary drives). With a better appreciation of the capabilities of linear drives it is likely that new markets for these machines will be developed. Consequently, there is a need for efficient computer-aided design tools that will allow a linear machine to be designed to meet the specifications for a transportation drive or for other industrial applications. It is proposed that a two-dimensional electromagnetic analysis, leading to an equivalent circuit of the machine for performance evaluation, and a two-dimensional finite-element analysis can together provide the information required for design purposes.

Paper LTC 85-008, approved by the Land Transportation Committee of the IEEE Industry Applications Society for presentation at the 1985 Industry Applications Society Annual Meeting, Toronto, ON, Canada, October 6–11. This work supported in part by the Natural Sciences and Engineering Research Council of Canada, in part by the Transport Canada Transportation Development Centre, and in part by the Urban Transportation Development Corporation. Manuscript received November 26, 1985.

G. E. Dawson and A. R. Eastham are with the Department of Electrical Engineering, Queens University, Kingston, ON, Canada K7L 3N6.

J. F. Gieras is with the Department of Electrical Machines and Drives, the Academy of Technology and Agriculture, Al. S. Kaliskiego 7, 85-763 Bydgoszcz, Poland.

R. K. I. Ong is at 12 Lorong 5, Realty Park, Singapore 1954.

K. Ananthasivam is with Infosys Consultants (PVT) Limited, 7th Main, 5th Block, Jayanagar, Bangalore, India 560041.

IEEE Log Number 8609008.

II. Electromagnetic Analysis

A transverse section of the single-sided LIM to be analyzed is shown in Fig. 2. Calculation of the field in a two-dimensional longitudinal section of the LIM has been shown to be entirely adequate for engineering performance evaluation [1], [2]. Transverse edge and longitudinal end effects are accounted for by well-established correction factors.

For analytical purposes, the LIM is modeled as shown in Fig. 3. The primary core is assumed to have infinite permeability and zero conductivity (i.e., laminated). The winding is represented by a current sheet containing the original space harmonics. The actual gap g is multiplied by Carter's coefficient k_c and by a saturation factor $k_\mu (g' = k_c k_\mu g)$ to account for primary slotting and saturation in the magnetic circuit. The double-layer reaction rail comprises a high-conductivity cap over a ferromagnetic core, which may, in general, be solid steel.

In this two-dimensional analysis, excitation currents flow in only the y direction, and the magnetic field has only two components: B_x parallel, and B_z perpendicular, to the direction of motion x. The electromagnetic field distribution in the LIM may then be described by equations in series form, which take into account skin effect and the reaction of secondary induced currents on the airgap field. These equations are given in simplified form in the Appendix.

In general, space harmonics [2] and both time harmonics and phase unbalance [3] should be taken into account. However, it has been shown that the effect of space harmonics in an LIM is small (producing, at most, a 5-percent change in thrust and normal forces for a machine with appropriately chorded windings) [2] and that the effect of time harmonics is negligible [3]. Therefore, for the purpose of this paper, it is adequate to present equations for fundamental space and time harmonics only, to illustrate the analytical approach. The more general equations may be found in [1]–[3].

Saturation and hysteresis effects in a solid steel core are included by postulating a complex equivalent relative permeability of solid steel μ_{re} [2], [4]:

$$\mu_{re} = \mu_{rs}(\mu' - j\mu'') \tag{1}$$

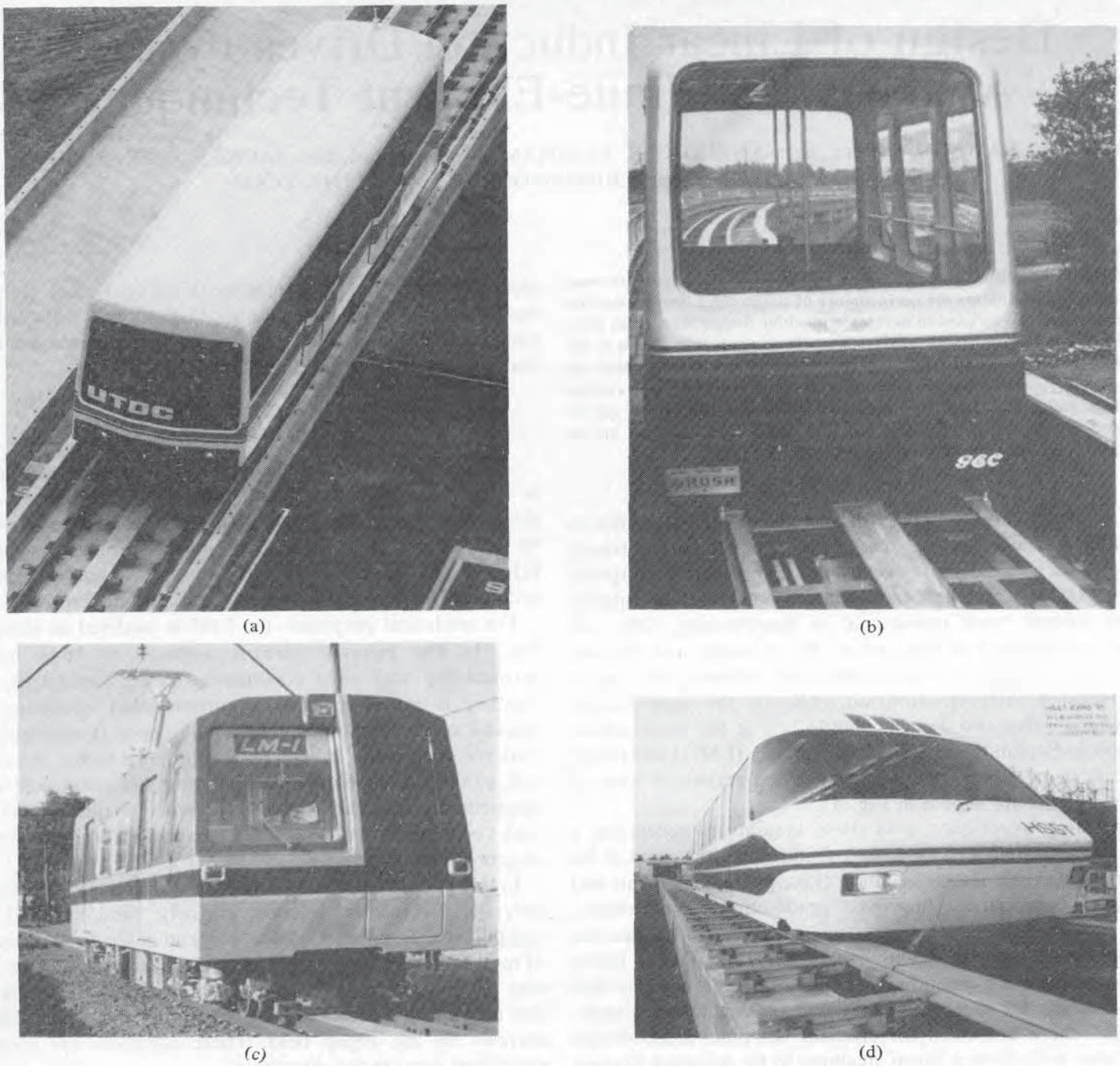

(a) (b) (c) (d)

Fig. 1. Linear induction motor-driven vehicle systems. (a) UTDC's intermediate-capacity transit system. (b) Advanced Transit Shuttle, linking Birmingham Airport and the National Exhibition Centre in England. (c) Hitachi's prototype mini-subway vehicle. (d) Japan Air Lines' HSST-03 vehicle, as demonstrated at EXPO '85 in Tsukuba, Japan.

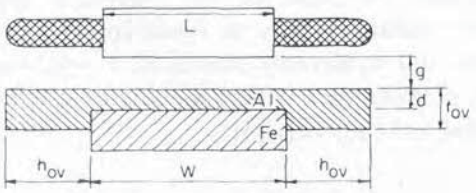

Fig. 2. Transverse section of a single-sided LIM with double-layer secondary.

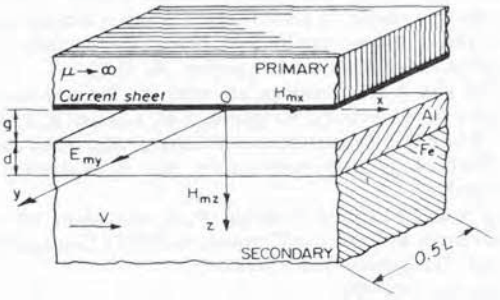

Fig. 3. Model of single-sided LIM for development of electromagnetic field equations.

where μ_{rs} is the surface value of relative permeability, and the real and imaginary components, μ' and μ'', respectively, are derived in [4].

The saturation factor for the magnetic circuit, used as a multiplier to obtain the equivalent airgap in the LIM model, is given by

$$k_\mu = \frac{V}{2(V_g + V_d)} \tag{2}$$

where V is the total MMF per pole pair, and V_g and V_d are the magnetic potential drops across the airgap and across the high-conductivity layer, respectively [2].

Transverse-edge effects (i.e., the longitudinal closure of induced currents in the side bar and core geometry of Fig. 2) are accounted for by correction factors. A modified Russell–Norsworthy factor [2] k_{RN} is used for the top cap, for which the corrected conductivity σ'_{Al} becomes

$$\sigma'_{Al} = k_{RN}\sigma_{Al}, \qquad k_{RN} < 1. \tag{3}$$

Many methods for treating transverse-edge effects in solid steel cores have been proposed, and we consider the correction factors due to Gibbs [5], Panasienkov [6], and Yee [7] to be the most generally applicable. The corrected core conductivity σ'_{Fe} becomes

$$\sigma'_{Fe} = \sigma_{Fe}/\bar{k}, \qquad \bar{k} > 1 \tag{4}$$

where $\bar{k}$ is taken to be the mean of the above three factors [5]–[7].

The most convenient method for accounting for longitudinal end effects is also by means of a correction factor [8] defined as

$$k_e = E_{me}/E_{ms} \tag{5}$$

where E_{ms} is the peak EMF induced in a primary phase winding by the magnetic wave traveling with synchronous velocity, and E_{me} is the peak EMF induced by the damped entry-end wave [9].

An analytical expression for this end-effect factor has been developed in terms of design parameters of a linear induction motor, and it has been validated by comparison with test results from one low-speed and one high-speed LIM [8], [10], [11]. This end-effect factor is used to modify the airgap voltage of the machine, as indicated in the per-phase equivalent circuit of Fig. 4.

With regard to the equivalent circuit, unit secondary impedance is given by the ratio of the tangential electric and magnetic field components at the surface of the reaction rail:

$$z_y = \left.\frac{E_{my2}}{H_{mx2}}\right|_{\text{at } z=g'} \equiv z_1 \cdot z_{12} \tag{6}$$

where z_1 is the unit impedance of the solid steel core given by

$$z_1 = -\frac{j\omega\mu_0\mu_{re}}{\kappa_1}$$

and z_{12} is the unit equivalent impedance of the high-conductivity layer, which is dependent on the parameters of the steel core and which is given by

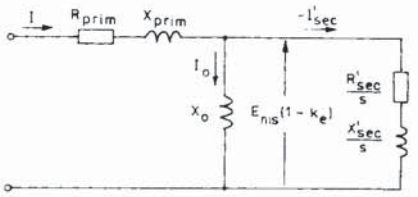

Fig. 4. Simplified per-phase equivalent circuit of LIM.

$$z_{12} = \frac{-\dfrac{j\omega\mu_0}{z_1\kappa_2}\sinh\ \kappa_2 d + \cosh\ \kappa_2 d}{\cosh\ \kappa_2 d - \dfrac{\kappa_2}{j\omega\mu_0} z_1 \sinh\ \kappa_2 d} \tag{7}$$

where $\omega = s\omega_1 = 2\pi f_1 s_1$ and f_1 is the input frequency. If $z_1 \to \infty$, the unit impedance of the secondary $z_y = z_1 \cdot z_{12} \to z_2$, and the unit impedance of the aluminum cap may then be derived as

$$z_2 = \frac{-j\omega\mu_0}{\kappa_2 \tanh\ \kappa_2 d}. \tag{8}$$

Secondary impedance referred to the primary winding is then

$$Z_{sec} = z_1 \cdot z_{12} \cdot 6L(Nk_w)^2/p\tau. \tag{9}$$

The impedance of the secondary branch of the T-type equivalent circuit, as shown in Fig. 4, can now be expressed as

$$\frac{Z_{sec}}{s} = \frac{R_{sec}}{s} + j\frac{X_{sec}}{s} = \frac{z_1 z_2}{z_1 + z_2} \cdot \frac{6L(Nk_w)^2}{p\tau s} \tag{10}$$

where s is the slip and L is the width of the LIM.

To calculate the magnetizing reactance, the unit impedance below the current sheet may be considered

$$z = \left.\frac{E_{my3}}{H_{mx3}}\right|_{\text{at } z=0} \equiv z_1 \cdot z_{12} \cdot z_{123} = z_y \cdot z_{123}$$

where

$$z_{123} = \frac{-\dfrac{j\omega_1\mu_0}{z_y\beta}\sinh\ \beta g' + \dfrac{1}{s}\cosh\ \beta g'}{\cosh\ \beta g' - \dfrac{\beta}{j\omega_1\mu_0} z_y \sinh\ \beta g'}. \tag{11}$$

If $z_y \to \infty$, the unit magnetizing reactance may be determined as

$$x_m = \frac{\omega_1\mu_0}{\beta \tanh\ \beta g'} \simeq \frac{\omega_1\mu_0}{\beta^2 g'} \tag{12}$$

Magnetizing reactance referred to the primary winding is therefore

$$X_m = \frac{\omega_1\mu_0}{\beta^2 g'} \cdot \frac{6L(Nk_w)^2}{p\tau}. \tag{13}$$

Note that the component of magnetizing current due to the high-conductivity layer is included in secondary impedance. Also, the magnetizing impedance would be modified if the primary core has significant losses [2].

For the equivalent circuit of Fig. 4, the secondary current referred to the primary winding is

$$I_{sec} = \frac{E_{ms}(1-k_e)}{\sqrt{(R_{sec}/s)^2 + (X_{sec}/s)^2}}. \tag{14}$$

Electromagnetic thrust then becomes

$$F_x = 3I_{sec}^2 R_{sec}/sv_s. \tag{15}$$

The normal force F_z consists of an attractive component F_{za} and a repulsive component F_{zr}. The attractive force is given by

$$F_{za} = \frac{1}{2\mu_0} B_{mzg}^2 p\tau L \tag{16}$$

where

$$B_{mzg} = \frac{\sqrt{2}E_{ms}(1-k_e)}{4fNk_w\tau L}.$$

Because F_x is proportional to B_{mzg}, and F_{zr} is proportional to B_{mxg}, the induced current reaction (repulsive) force can be equated to

$$F_{zr} = F_x B_{mxg}/B_{mzg} \tag{17}$$

with

$$B_{mxg} = \left| -\frac{A_m\mu_0}{\beta M}\left[\kappa_1 \cosh \kappa_2 d + \kappa_2\mu_{re} \sinh \kappa_2 d\right]\right|.$$

This model of the LIM, in which two-dimensional field analysis with transverse edge and longitudinal end effect factors is used to develop an equivalent circuit model of the machine, may therefore be used for computation of thrust and normal forces and, with the evaluation of primary resistance and leakage reactance, for determination of terminal characteristics.

Programs based on this model have been implemented on both VAX 11/750 and IBM-compatible personal computers, and have been validated [8] by comparing computed and experimental results for two large-scale LIM's; one tested at Queen's University [1]–[3], [10] and one tested by the General Electric Company [11]. Both test facilities use rotating wheels to provide relative motion between rim-mounted components (solid steel with aluminum cap) and a stationary vehicle module (the LIM primary). Design data for the Queen's University LIM are listed in Table I.

As an example, the thrust and normal forces for the Queen's University LIM are shown in Fig. 5. Similar good agreement is found between analysis and test results over a range of operating conditions ($5 < f < 60$ Hz; $10 < g < 20$ mm; $100 < I < 250$ A) and for different secondary top cap configurations ($0 < h_{ov} < 45$ mm), thus justifying the use of the model as an effective tool for LIM performance evaluation.

TABLE I
QUEEN'S TEST LIM DESIGN DATA

No. of phases	3
No. of pole pairs p	3
Pole pitch τ	0.25 m
No. of slots per pole per phase	3
Primary coil pitch	(7/9) 0.1944 m
Nominal input current I	200 A
Width of primary stack L	0.101 m
Nominal airgap g	15 mm
Thickness of aluminum cap d	2.5 and 4.5 mm
Width of overhang h_{ov}	34 mm
Thickness of overhang t_{ov}	9.5 mm
Width of solid back iron w	0.111 m

III. Finite-Element Analysis

As a result of analytical developments over the past ten years, the finite-element technique is now recognized as a powerful method for the evaluation of fields in electromagnetic machines and devices, and has been used by the authors to determine the time-dependent field distribution in a two-dimensional longitudinal section of the LIM.

For the solution of a two-dimensional field, the vector potential A normal to the plane of analysis is given by the partial differential equation

$$\nabla \times \frac{1}{\mu_0\mu_r} \cdot \nabla \times A = -J_s + \sigma \frac{\partial A}{\partial t} - \sigma v \times \nabla \times A \tag{18}$$

where μ_r is the relative permeability (which will be a nonlinear function of field intensity in ferromagnetic materials), σ is the local conductivity, J_s is the source current density, and v is the velocity.

The generalized time-domain solution can be determined by minimization of an energy functional formulated from the above equation, expressed in variational terms over the discretized plane. With regard to the right-hand side of (18), inclusion of the source term alone yields the Laplace equation and a magnetostatic solution for time-invariant systems. The second term accounts for transformer effects (i.e., due to time-varying fields in static systems), while the third term accounts for motional effects (i.e., in dynamic systems). The finite-length LIM is a dynamic system and, to evaluate the speed-dependent field distribution, all three terms must be included in the finite-element solution [12]–[14].

A two-dimensional longitudinal section of the Queen's University test LIM has been analyzed in this manner, using the fundamental time harmonic method in which time differentials are replaced by $j\omega$. The complete machine geometry has been modeled by a 2650 node mesh. One example of the resultant field distribution, showing equivector potentials, is presented in Fig. 6.

To validate the finite-element field solution, the computed distribution of normal flux density in the airgap has been compared with test results measured by a sequence of airgap search coils under various dynamic conditions. Three such comparisons are shown in Fig. 7. The space waves represent the instantaneous finite-element solution, while the test results are shown in terms of the peak field attained during a complete

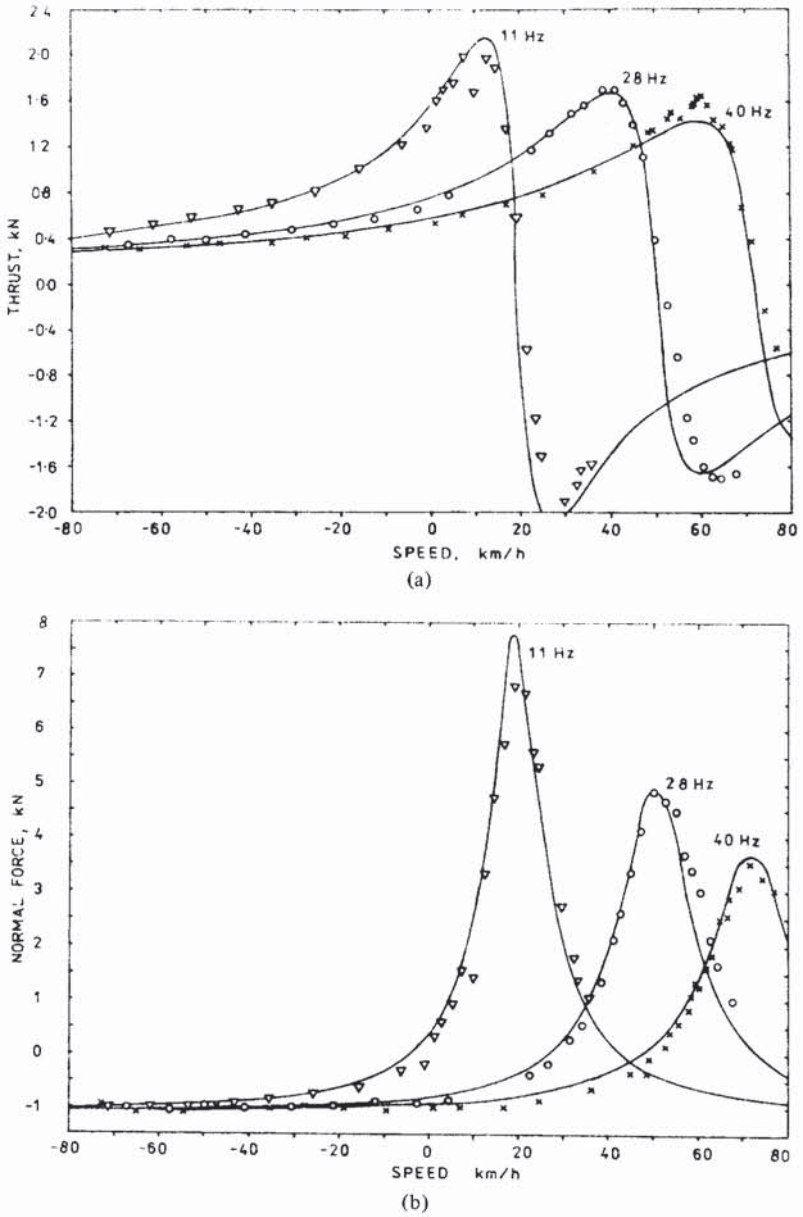

Fig. 5. Electromagnetic analysis and test results for (a) thrust and (b) normal force, as functions of speed for the Queen's test LIM at various fixed frequencies, with $I = 200$ A, $d = 4.5$ mm, at $g = 15$ mm.

ac cycle. Very good agreement is evident. The three sets of results in Fig. 7 are for synchronous speeds at frequencies of 11, 28, and 40 Hz, and clearly show the enhancement of longitudinal end effect at higher speed, i.e., the delay in the establishment of airgap flux at the front end of the machine due to parasitic eddy currents in the reaction rail.

The finite-element solution may be stepped incrementally through an ac cycle to determine the peak flux density at any point in the LIM. In this manner the primary lamination and secondary core designs may be iteratively optimized to give the best performance–weight ratio for the LIM.

An attempt has been made to evaluate the LIM thrust and normal forces by the finite-element method, as shown in Fig. 8. It may be noted that, while the shape- and speed-dependences of the analytical and test data are similar, the finite-element curves are lower than the test results, particularly near peak-motoring thrust. Similar results were noted in [14]. The only correction factors that were used for analytical purposes were to apply 1) the modified Russell–Norsworthy factor to the aluminum cap conductivity as in (3), and 2) a factor of 1.1 to account for the secondary core being 10-percent wider than the primary stack. In view of the better results achievable with electromagnetic analysis, this technique is considered to provide the most reliable calculation of thrust and normal forces and terminal characteristics.

IV. Conclusion

In this paper we have presented a review of two analytical techniques that are complementary in evaluating the performance of an LIM and that can be used for computer-aided design purposes. For more complete details of the general electromagnetic equations and their development, the reader is

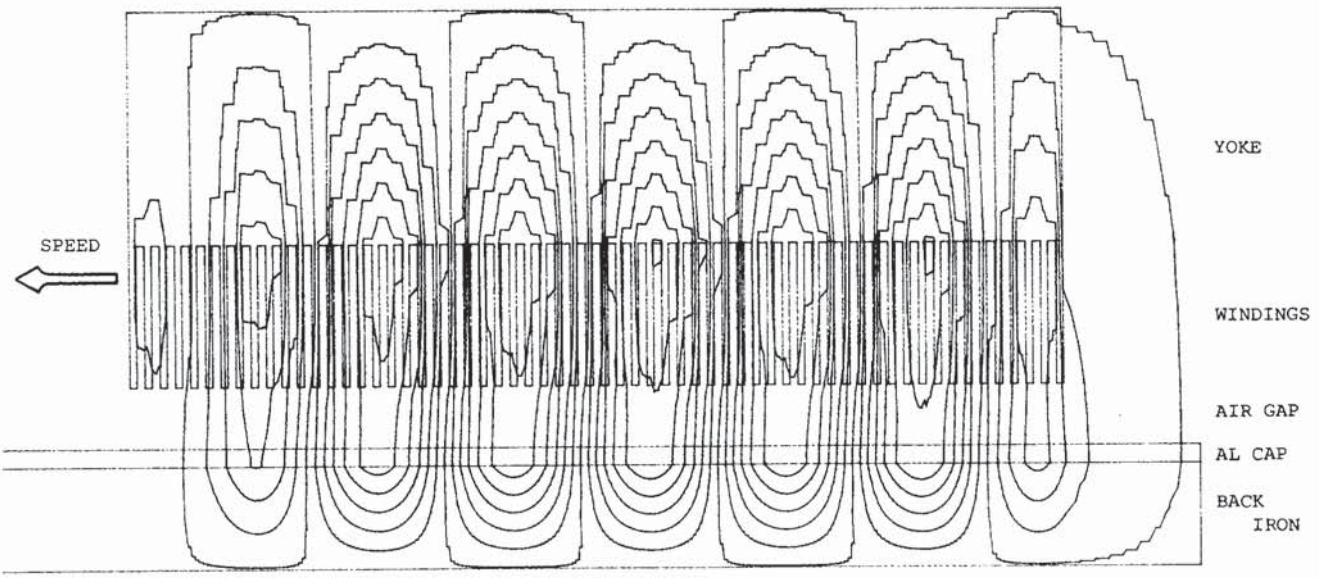

Fig. 6. Field distribution in Queen's test LIM as determined by finite elements, with $I = 200$ A, $d = 4.5$ mm, $g = 15$ mm, $f = 11$ Hz, $v = 7.2$ km/h (i.e., slip frequency = 7 Hz; close to peak in thrust-speed curve), with equipotentials plotted at $\Delta A = 0.004$ Wb/m. Note horizontal axis has been contracted relative to vertical axis for presentation purposes.

referred to [1]–[4], and [8]. It has been shown that a two-dimensional electromagnetic technique with transverse edge and longitudinal end effect corrections can be used to obtain force and terminal characteristics to sufficient accuracy for engineering design purposes. The finite-element method then provides detailed information about the field distribution in the machine. Taken together, both techniques allow an optimal electromagnetic design for an LIM to be iteratively developed.

Appendix

Electromagnetic Field Equations

The simplified two-dimensional electromagnetic field equations considering only the fundamental space and time harmonics may be expressed in the following form [1], [2].

A) For $0 < z < g'$ (i.e., in the airgap)

$$H_{mx3} = -\frac{A_m e^{-j\beta x}}{M}\left\{\frac{\kappa_2}{\beta}\left[\frac{\kappa_1}{\kappa_2}\cosh\ \kappa_2 d + \mu_{re}\sinh\ \kappa_2 d\right]\cdot\cosh\ \beta(z-g') - \left[\mu_{re}\cosh\ \kappa_2 d + \frac{\kappa_1}{\kappa_2}\sinh\ \kappa_2 d\right]\cdot\sinh\ \beta(z-g')\right\} \quad (A.1)$$

$$H_{mz3} = \frac{jA_m e^{-j\beta x}}{M}\left\{\left[\mu_{re}\cosh\ \kappa_2 d + \frac{\kappa_1}{\kappa_2}\sinh\ \kappa_2 d\right]\cdot\cosh\ \beta(z-g') - \frac{\kappa_2}{\beta}\left[\frac{\kappa_1}{\kappa_2}\cosh\ \kappa_2 d + \mu_{re}\sinh\ \kappa_2 d\right]\cdot\sinh\ \beta(z-g')\right\} \quad (A.2)$$

$$E_{my3} = \frac{j\omega\mu_0 A_m e^{-j\beta x}}{\beta M}\left\{\left[\mu_{re}\cosh\ \kappa_2 d + \frac{\kappa_1}{\kappa_2}\sinh\ \kappa_2 d\right]\cdot\cosh\ \beta(z-g') - \frac{\kappa_2}{\beta}\left[\frac{\kappa_1}{\kappa_2}\cosh\ \kappa_2 d + \mu_{re}\sinh\ \kappa_2 d\right]\cdot\sinh\ \beta(z-g')\right\}. \quad (A.3)$$

B) For $g' < z < d + g'$ (i.e., in the high-conductivity layer)

$$H_{mx2} = -\frac{A_m \kappa_2 e^{-j\beta x}}{M\beta}\left\{\frac{\kappa_1}{\kappa_2}\cosh\ \kappa_2(z-d-g') - \mu_{re}\sinh\ \kappa_2(z-d-g')\right\} \quad (A.4)$$

$$H_{mz2} = \frac{jA_m e^{-j\beta x}}{M}\left\{\mu_{re}\cosh\ \kappa_2(z-d-g') - \frac{\kappa_1}{\kappa_2}\sinh\ \kappa_2(z-d-g')\right\} \quad (A.5)$$

$$E_{my2} = \frac{j\omega\mu_0}{\beta M} A_m e^{-j\beta x}\left\{\mu_{re}\cosh\ \kappa_2(z-d-g') - \frac{\kappa_1}{\kappa_2}\sinh\ \kappa_2(z-d-g')\right\}. \quad (A.6)$$

C) For $z > d + g'$ (i.e., in the solid steel secondary core)

$$H_{mx1} = -\frac{\kappa_1 A_m}{M\beta} e^{-j\beta x} e^{-\kappa_1(z-d-g')} \quad (A.7)$$

$$H_{mz1} = \frac{jA_m}{M} e^{-j\beta x} e^{-\kappa_1(z-d-g')} \quad (A.8)$$

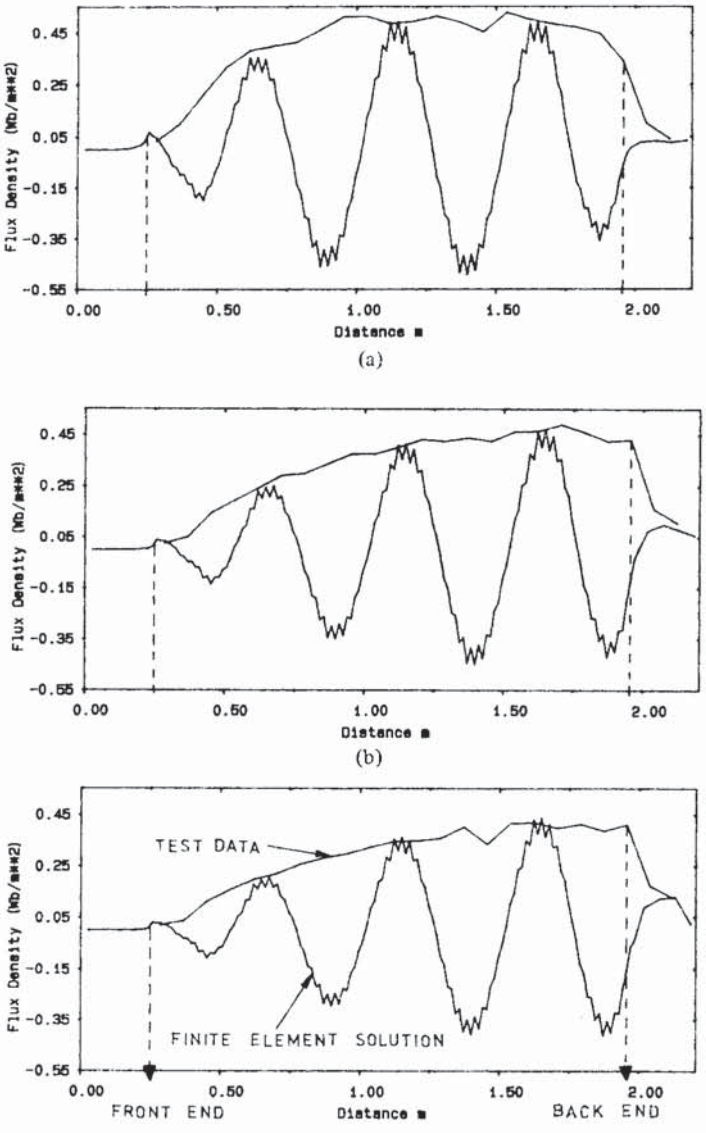

Fig. 7. The field distribution along the airgap of the Queen's test LIM, with $I = 200$ A, $d = 4.5$ mm, $g = 15$ mm, at synchronous speeds: (a) $f = 11$ Hz, $v = 19.8$ km/h; (b) $f = 28$ Hz, $v = 50.4$ km/h; (c) $f = 40$ Hz, $v = 72$ km/h.

$$E_{my1} = \frac{j\omega\mu_0\mu_{re}A_m}{M\beta} e^{-j\beta x} e^{-\kappa_1(z-d-g')} \tag{A.9}$$

where

$$M = \frac{\kappa_2}{\beta}\left[\frac{\kappa_1}{\kappa_2}\cosh\ \kappa_2 d + \mu_{re}\sinh\ \kappa_2 d\right] \cdot \cosh\ \beta g' + \left[\mu_{re}\cosh\ \kappa_2 d + \frac{\kappa_1}{\kappa_2}\sinh\ \kappa_2 d\right]\sinh\ \beta g'.$$

Also

$$\beta = \frac{\pi}{\tau} \qquad \kappa_1 = \sqrt{\alpha_1^2 + \beta^2} \qquad \kappa_2 = \sqrt{\alpha_2^2 + \beta^2} \tag{A.10}$$

where the propagation constants are given by

$$\alpha_1 = \sqrt{j\omega\mu_0\mu_{re}\sigma'_{Fe}} \qquad \alpha_2 = \sqrt{j\omega\mu_0\sigma'_{Al}}\,. \tag{A.11}$$

(A.1)-(A.9) should also include the fundamental time harmonic factor $e^{j\omega t}$.

For a three-phase machine the peak value of fundamental space harmonic of primary current density is

$$A_m = \frac{3\sqrt{2}k_w NI}{p\tau}\ (\text{A/m}) \tag{A.12}$$

where N is the number of primary turns per phase, k_w is the winding factor, p is the number of pole pairs, τ is the pole pitch, and I is the primary current.

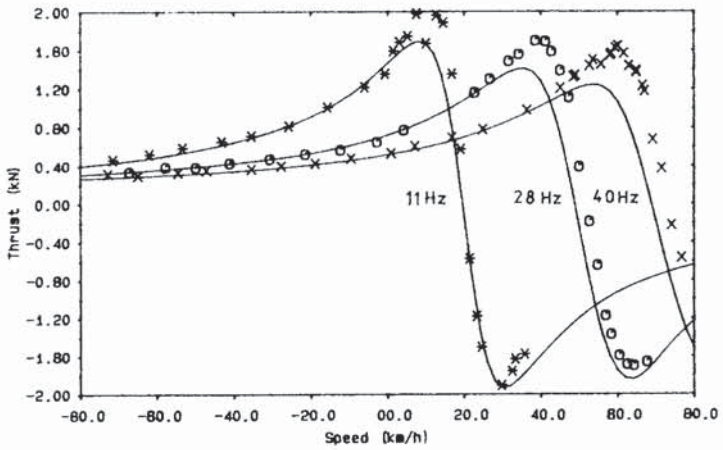

(a)

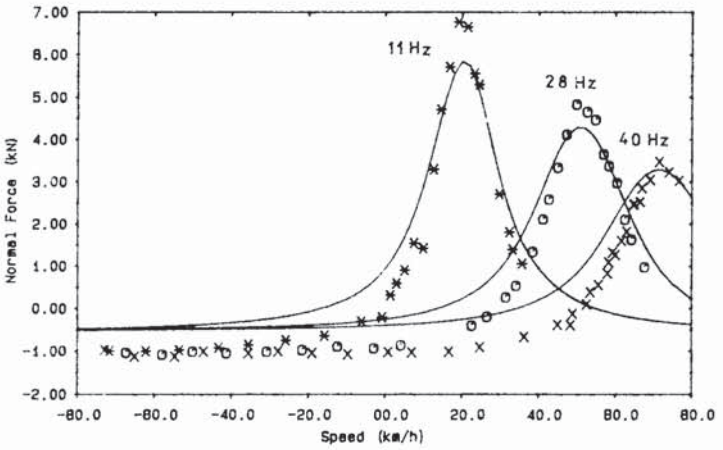

(b)

Fig. 8. Finite element analysis and test results for (a) thrust and (b) normal force, as functions of speed for Queen's test LIM at various fixed frequencies, with I = 200 A, d = 4.5 mm, at g = 15 mm.

References

[1] J. F. Gieras, A. R. Eastham, and G. E. Dawson, "Performance calculation for single-sided linear induction motors with a solid steel reaction plate under constant current excitation," Part B, accepted for publication in *Proc. IEE*, Part B, vol. 132, no. 4, 1985, pp. 185-194.

[2] J. F. Gieras, G. E. Dawson, and A. R. Eastham, "Performance calculation for single-sided linear induction motors with a double-layer reaction rail under constant current excitation," submitted for publication in *IEEE Trans. Magn.*, MAG-22, no. 1, 1986, pp. 54-62.

[3] J. F. Gieras, A. R. Eastham, G. E. Dawson, and G. John, "Calculation of thrust for a single-sided linear induction motor, taking into account phase unbalance and higher time harmonics," Part B, submitted for publication in *Proc. IEE*, 1985.

[4] J. F. Gieras, "Analytical method of calculating the electromagnetic field and power losses in ferromagnetic halfspace, taking into account saturation and hysteresis," *Proc. IEE*, vol. 124, no. 11, 1977, pp. 1098-1104.

[5] W. J. Gibbs, "Theory and design of eddy current slip couplings," *British Electrical and Allied Manufacturers Assn. J*, vol. 53, pp. 123, 172-7, 219, 1946.

[6] M. A. Panasienkov, "Electromagnetic calculations of devices with nonlinear distributed parameters," *Energia*, Moscow, 1971 (in Russian).

[7] H. Yee, "Effects of finite length in solid-rotor induction machines," *Proc. IEE*, vol. 118, no. 8, 1971, pp. 1025-1033.

[8] J. F. Gieras, G. E. Dawson, and A. R. Eastham, "A new longitudinal end effect factor for linear induction motors," accepted for publication in *IEEE Trans. Power App. Syst.*, Paper no. 86 WM 209-1, presented at IEEE/PES 1986 Winter Meeting, New York, NY.

[9] S. Yamamura, *Theory of Linear Induction Motors*. New York: John Wiley, 1972.

[10] A. R. Eastham, G. E. Dawson, D. M. Pringle, and J. M. Davidson, "Comparative experimental evaluation of the performance of a SLIM with a solid-steel reaction rail and with an aluminum capped reaction rail," CIGGT Report No. 80-7, Queen's University, Kingston, ON, Canada, 1980.

[11] G. B. Kliman, W. R. Mischler, and W. R. Oney, "Performance of a single-sided linear induction motor with solid back iron and with various misalignments," Report No. FRA/ORD-80/53-1, GEC, Schenectady, New York, 1980.

[12] M. V. K. Chari, "Finite element solution of the eddy current problem in magnetic structures," *IEEE Trans. Power App. Syst.*, PAS-93, pp. 62-72, 1973.

[13] A. Foggia, J. C. Sabonnadiere, and P. Silvester, "Finite element solution of saturated travelling magnetic field problems," *IEEE Trans. Power App. Syst.*, PAS-94, pp. 866-71, 1975.

[14] J. H. H. Alwash and J. A. H. Al-Rikabi, "Finite element analysis of linear induction machines," in *Proc. IEE*, vol. 126, no. 7, 1979, pp. 677-82.

Graham E. Dawson (S'66–M'69) was born in North Vancouver, BC, on November 11, 1939. He received his B.A.Sc., M.A.Sc., and Ph.D. degrees from the University of British Columbia in 1963, 1966, and 1970, respectively.

In 1969 he joined the Department of Electrical Engineering, Queen's University at Kingston as an Assistant Professor. He was promoted to Associate Professor in 1975, and to Professor in 1981. His electrical engineering research activities have been associated with the transportation industry, and he has current interest in the computer-aided design and performance of rotary and linear traction motors and energy management of transportation systems.

Dr. Dawson is a Registered Professional Engineer in the Province of Ontario and a member of the Canadian Society for Electrical Engineering.

Anthony R. Eastham (M'75–SM'83) received the B.Sc. degree in physics from the University of London in 1965, and the Ph.D. degree from the University of Surrey in 1969.

After research work at Plessey Telecommunications Limited and at the University of Warwick, he joined the Canadian Institute of Guided Ground Transport, where he coordinated a group that technically defined, component tested, and assessed high-speed Maglev in Canada. He is now a Professor of electrical engineering at Queen's University in Kingston, ON, Canada, having joined the faculty in 1978. His research activities include innovative urban and high-speed transportation, linear electric drives, and electromagnetic analysis.

Dr. Eastham is a Registered Professional Engineer in the Province of Ontario.

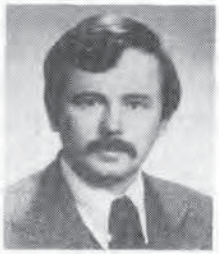

Jacek F. Gieras (M'83) was born in [redacted] on [redacted]. He received the M.Sc. (Mgr.inz.) degree in electrical engineering from the Technical University of Lodz, the Ph.D. (Dr.inz.) and D.Sc. (Dr.hab.) degrees, also in electrical engineering, from the Technical University of Poznan (Poland) in 1971, 1975, and 1980, respectively.

His research activities include analysis of electromagnetic fields in electrical machines and devices, computer-aided design of electrical machines, magnetic levitation, and industrial drives. He is a co-author of the monograph *Induction Machines with Solid Rotor*, issued by the Polish Scientific Publishing House in 1977, author of the textbook *Special Purpose Electric Machines* (ATR Bydgoszcz, 1983), and author of 70 scientific papers published in many countries, including the United Kingdom, the US, West Germany, and Japan. From November 1983 until September 1985 he was a Visiting Associate Professor in the Department of Electrical Engineering at Queen's University, Kingston, ON, Canada. At present, he is Associate Professor in the Department of Electrical Machines and Drives at the Academy of Technology and Agriculture, Bydgoszcz, Poland.

Raymond K. I. Ong graduated from Southampton University in the UK and received the B.Sc. (Hons.) degree in electrical engineering in 1981. He received the M.Sc. degree in electrical engineering from Queen's University, Kingston, ON, Canada in 1984.

His areas of research activity are in finite element analysis of electromagnetic devices, electrical machines, guided ground transportation, power systems, and power electronics.

Krishnamoorthy Ananthasivam was born on April 10, 1961 in South India. He received the B.Tech. degree in electrical engineering from the Indian Institute of Technology, Madras, India, in 1983. He received the M.Sc. (Eng.) degree in electrical engineering from Queen's University, Kingston, ON, Canada in 1985.

His current interests are in the area of software development for engineering applications, and he is currently employed as a Software Engineer in South India.